RSC Advances

PAPER

View Article Online
View Journal | View Issue



Cite this: *RSC Adv.*, 2023, **13**, 10397

# Enhanced adsorption capacity of tetracycline on porous graphitic biochar with an ultra-large surface area†

Bingyuan Huang,[a] Dan Huang,[b] Qian Zheng,[a] Changhan Yan,[a] Jiaping Feng,[a] Hejun Gao, *[a] Hongquan Fu *[a] and Yunwen Liao*[a]

Received 3rd February 2023
Accepted 23rd March 2023

DOI: 10.1039/d3ra00745f

rsc.li/rsc-advances

Excessive tetracycline in the water environment may lead to the harming of human and ecosystem health. Removing tetracycline antibiotics from aqueous solution is currently a most urgent issue. Porous graphitic biochar with an ultra-large surface area was successfully prepared by a one-step method. The effects of activation temperature, activation time, and activator dosage on the structural changes of biochar were investigated by scanning electron microscopy, Brunauer–Emmett–Teller, X-ray powder diffraction, and Raman spectroscopy. The effect of the structure change, adsorption time, temperature, initial pH, and co-existing ions on the tetracycline removal efficiency was also investigated. The results show that temperature had the most potent effect on the specific surface area, pore structure, and extent of graphitization. The ultra-large surface area and pore structure of biochar are critical to the removal of tetracycline. The $q_e$ of porous graphitic biochar could reach 1122.2 mg $g^{-1}$ at room temperature. The calculations of density functional theory indicate that π–π stacking interaction and p–π stacking interaction can enhance the tetracycline adsorption on the ultra-large surface area of graphitic biochar.



## 1 Introduction

Since antibiotics are widely used in treating and preventing human and animal diseases, they have significantly improved human and animal health.[1] Tetracycline (TC) is the second largest antibiotic in the world and is usually used as a feed additive to improve the growth efficiency of animals to fight bacterial infections.[2] However, residual TC can cause drug resistance in bacteria and alter the ecological function of microorganisms. It has seriously endangered the safety of drinking water and directly posed a threat to human health.[3] Many technologies have been applied to remove the TC from water, such as membrane technology,[4] adsorption,[5] and degradation.[6] In these technologies, the adsorption method is widely used in removing TC because of its high efficiency, low cost, and simplicity.[7,8] The selection of an efficient adsorbent is critical to enhancing the adsorption capacity of TC. Raw activated carbon has been used to remove TC.[9,10] However, poor adsorption capacity restricts its practical application.[11] Biochar is produced from biomass, which is abundant worldwide, renewable, inexpensive, and environmentally friendly.[12] It is excellent potential to remove TC.

The application of biochar prepared from different biomass to remove TC has attracted extensive attention from scholars, such as alfalfa,[13] bovine manure,[14] maple leaf,[15] and sludge,[16] which exhibit excellent adsorption performance. The mechanisms responsible for TC adsorption by biochar could be assigned to hydrogen bonding, π–π interaction, and electrostatic.[17] For example, Hussam *et al.*[18] suggested that hydrogen bonding and π–π electron–acceptor–donor interactions are two fundamental adsorption mechanisms of the biochar from excess food and garden materials. They had an adsorption capacity between 2.98 mg $g^{-1}$ and 8.23 mg $g^{-1}$ for initial TC concentrations of 20 mg $L^{-1}$ and 100 mg $L^{-1}$, respectively. The mechanism of TC adsorption on rice straw-derived biochar mainly included physical adsorption, electrostatic interaction, hydrogen bonding, and π–π interaction, with the maximum adsorption capacity could reach 103 mg $g^{-1}$.[19] However, many pristine biochars have a low specific surface area, poorly formed pores, and graphitic structures.[20] which leads to low adsorption performance ($Q_e$ < 150 mg $g^{-1}$) without the possibility of practical application.[9,18]

In order to solve the structural problem of pristine biochar with low adsorption capacity, chemical activation has been used in the preparation process of biochar with ultra-surface area for exposing more adsorption sites. The material has an ultra-high specific surface area, which helps to improve its practical application performance-for example, the adsorption of iodine

[a]*Chemical Synthesis and Pollution Control Key Laboratory of Sichuan Province, Institute of Applied Chemistry, College of Chemistry and Chemical Engineering, China West Normal University, Nanchong, Sichuan 637000, China. E-mail: hejun_gao@126.com; fubestone@163.com; liao-yw@163.com*

[b]*People's Hospital of Gaoping District, Nanchong, Sichuan 637100, China*

† Electronic supplementary information (ESI) available. See DOI: https://doi.org/10.1039/d3ra00745f

and catalytic styrene.[21,22] Currently, biochar has been activated by $FeCl_3$,[23] $H_3PO_4$,[24] and NaOH[20] as the activating agent, to change its surface structure to improve the adsorption efficiency of TC. For example, Kan *et al.*[25] prepared NaOH-activated biochar with high adsorption performance by activating alfalfa with NaOH. The specific surface area of biochar increased from 0.68 $m^2\ g^{-1}$ to 796.50 $m^2\ g^{-1}$, and the adsorption performance of tetracycline was improved from 17.85 to 232.88 mg $g^{-1}$. The surface structure of biochar was markedly improved. However, biochar is inevitably post-treated with strong acid or strong alkali to remove the activating agent, increasing the process cost and second environmental pollution for adsorption TC. Therefore, there are two noteworthy points for selecting the activating agent in pyrolysis biomass: (1) easy to occur in the biochar surface reaction, increasing the pore structure and surface area. (2) No residue on the biochar surface, and easy to collect activating agents after the pyrolysis process. In this study, $ZnCl_2$ is selected as activator, and its pore-forming process is as follows. Firstly, when the temperature reaches about 400 °C, $ZnCl_2$ and $H_2O$ from the pyrolytic biomass start to transform to ZnO: $ZnCl_2 + H_2O \rightarrow ZnO + HCl$.[26,27] The pores formation begins after 600 °C. Secondly, the reaction of ZnO and the biochar from biomass form Zn and other gases. Lastly, in the process from liquid metal zinc to gaseous metal zinc at high temperature, porous can also be further made to increase the surface area of biochar, and metal Zn can be further collected: Zn (liquid) → Zn (gas).[28] Therefore, $ZnCl_2$ activating agents can prepare the porous and high surface area of biochar because there are two porous-making processes on biochar.

In this work, we select corn starch as the source of biochar because it is widely used and is an essential raw material in the food, chemical industry, medicine, and other industries. Especially there is a large surplus of genetically modified (GM) corn, and this work also can provide an application for GM corn.[29] Corn starch and $ZnCl_2$ can form a uniform mixture by the planetary ball mill machine to produce porous biochar by pyrolysis. The specific surface area, pore structure, and graphite degree of biochar were controlled by the activation temperature, dosage of $ZnCl_2$, and activation time. The adsorption efficiency of TC on porous biochar was evaluated, including the pH, adsorption time, concentration of TC, adsorption temperature, and coexisting ions. The adsorption mechanism between biochar and TC will be proposed. It will be a new path for further research on developing the high-adsorption performance of tetracycline on porous graphitic biochar with an ultra-large surface area.

# 2 Materials and methods

## 2.1 Materials

The corn starch, tetracycline (TC, $C_{22}H_{24}N_2O_8$), $ZnCl_2$, NaCl, NaOH, and Humic Acid (HA) were obtained from Aladdin Reagent Co., Ltd (Shanghai, China). $CaCl_2$, $NH_4Cl$, and $Na_2CO_3$ were purchased from Bailingwei Technology Co., Ltd (Beijing, China). $Na_2SO_4$ and HCl were supplied by Kelong Chemical Reagent Co., Ltd (Chengdu, China). All chemicals are analytical grade, and deionized water was used for all experiments.

## 2.2 Preparation of biochar

The porous biochar was prepared by one-step carbonization activation. Briefly, a certain proportion of starch and $ZnCl_2$ were put into the planetary ball mill machine, which was set at 300 rpm for 1 h. Then, the mixture was placed into a tubular furnace with an oxygen-deficient atmosphere for pyrolysis (40 mL $min^{-1}$ of $N_2$ flow), and the sample was calcined at 800 °C for 2 h (5.0 °C $min^{-1}$). After cooling down to room temperature, the black solid was washed with 2 M HCl solution several times and then washed with DI water until to neutrality. Finally, the obtained product was dried in an oven at 60 °C for 24 h. The biochar from the different samples was designated as $BC_{x\text{-}y\text{-}z}$, where $x$ represented the calcination time (h), $y$ was the calcination temperature (°C), and $z$ was the ratio of $ZnCl_2$ to starch. Firstly, the ratio and calcination time was fixed, and the calcination temperature was changed. Then the product was labeled $BC_{2\text{-}400\text{-}4}$, $BC_{2\text{-}600\text{-}4}$, $BC_{2\text{-}800\text{-}4}$, and $BC_{2\text{-}1000\text{-}4}$. Secondly, only changing the ratio of $ZnCl_2$ and corn starch, the sample was named $BC_{2\text{-}800\text{-}0.5}$, $BC_{2\text{-}800\text{-}1}$, $BC_{2\text{-}800\text{-}2}$, $BC_{2\text{-}800\text{-}4}$, and $BC_{2\text{-}800\text{-}6}$. Finally, just calcination time is 1, 2, ad 3, and the sample was named $BC_{1\text{-}800\text{-}4}$, $BC_{2\text{-}800\text{-}4}$, and $BC_{3\text{-}800\text{-}4}$. The materials are collectively referred to as BC, and the $BC_{800}$ is a sample without $ZnCl_2$ in the calcining process.

## 2.3 Characterization

The morphology of BC was observed by scanning electron microscopy (SEM, ZEISS G300, Germany). The specific surface area, the pore volume, and pore size data of BC were measured by Brunauer–Emmett–Teller (version 3.0, Quantachrome Instruments Ltd., USA). To characterize the chemical structure of BC, Fourier transforms infrared spectroscopy (FTIR, Thermo Nicolet Ltd., USA) was conducted. The crystal structures of BC were examined by an X-ray powder diffraction analyzer (XRD Ultima IV, Rigaku Ltd., Japan). Structural defects and graphitization of BC were carried out using a Raman microscope (alpha 300 access, WITec, Germany) with a 532 nm wavelength laser.

## 2.4 Batch adsorption

In this work, batch adsorption tests were conducted in a 50 mL glass colorimetric tube at 30 °C, and the mixture was stirred for 4 h. After adsorption, the solution was filtered with a 0.22 μm microporous membrane, and the residual concentration was measured by UV-vis spectrophotometer at $\lambda_{max} = 357$ nm (L6S, Shanghai Yidian Scientific Instrument Co., Ltd, China). More detailed experimental parameters such as pH, kinetics, isotherms, thermodynamics and ionic strength were designed as ESI (Table S1†).

The cycle experiment process was as follows. Take 100 mg adsorbent and 500 mL tetracycline for adsorption. After one adsorption, collected the biochar and washed with deionized water, then dried at 80 °C. The TC-loaded biochar was desorbed with 0.1 M NaOH solution for 12 h and repeated the above experiment 5 times in a turn. The calculation of adsorption capacity, removal efficiency, kinetics, isotherms, and thermodynamics were presented in ESI (Table S2†).

# 3 Results and discussion

## 3.1 Structure characterization

The effect of the activation conditions, such as temperature, time and the amount of the activator on the structure of $BC_{x\text{-}y\text{-}z}$ was investigated. Morphologies of the samples $BC_{x\text{-}y\text{-}z}$ were investigated by SEM (Fig. 1 and S1†).

$BC_{800}$ has a bulk morphology under high temperatures (Fig. S1a†). $BC_{2\text{-}400\text{-}4}$ and $BC_{2\text{-}600\text{-}4}$ exhibit similar morphologies and sizes (Fig. 1a and b) to $BC_{800}$ at activation temperatures of 400 °C and 600 °C, respectively. The results indicate that at lower activation temperatures, $ZnCl_2$ has a weaker effect on the surface morphology and pore-forming ability of the biochar. However, at activation temperature of 800 °C and above, the biochar surface exhibits a distinct porous structure (Fig. 1c and d), indicating that high temperatures are favorable for generating pores and porous surface structures by $ZnCl_2$ in biochar.[30]

The effect of activation time on the surface morphology of BC is shown in Fig. 1e and f. The porous surface cannot be obtained when the reaction activation time is 1 h at 800 °C. It is obvious that a shorter activation would not be beneficial to form a porous surface. When the reaction time is 2 h, the surface of the material exhibits a porous structure. However, the longer activation time *via* $ZnCl_2$ above 3 h will lead to the collapse of the channel or even millimeter-sized pore on $BC_{3\text{-}800\text{-}4}$ (Fig. 1f). The amount of $ZnCl_2$ will also affect the surface structure, the ratio of $ZnCl_2$/starch is lower than 2 : 1 at 800 °C, and the surface of the BC does not have porous structures in Fig. S1a–d.† Further increasing the ratio of $ZnCl_2$/starch will show an obvious porous structure on the biochar, indicating that the amount of $ZnCl_2$ can affect forming of the structure of the porous biochar with some millimeter-sized macropores.[31] Overall, starch was treated with $ZnCl_2$ (4 : 1, $ZnCl_2$/starch) for 2 h at 800 °C, and a porous surface of BC could be obtained. The presence of a porous structure can increase the surface area of biochar.

In order to further investigate the effect of porous structure on the surface of the BC, nitrogen adsorption–desorption isotherms were used to measure the specific surface area and pore structure of BC (Fig. 2, S2, S3, and Table S3†).

According to the IUPAC report,[32] the $BC_{800}$ in Fig. 3 exhibits a Type I isotherm (Fig. S2†), which is typically obtained from microporous materials.[33] Instead, $BC_{x\text{-}y\text{-}z}$ is observed in Fig. S2 and S3† to exhibit an ink bottle-like hysteresis loop, which is the H2 hysteresis loop for the Type IV(a) isothermal line.[32] This is generally observed in mesoporous materials with non-rigid pore

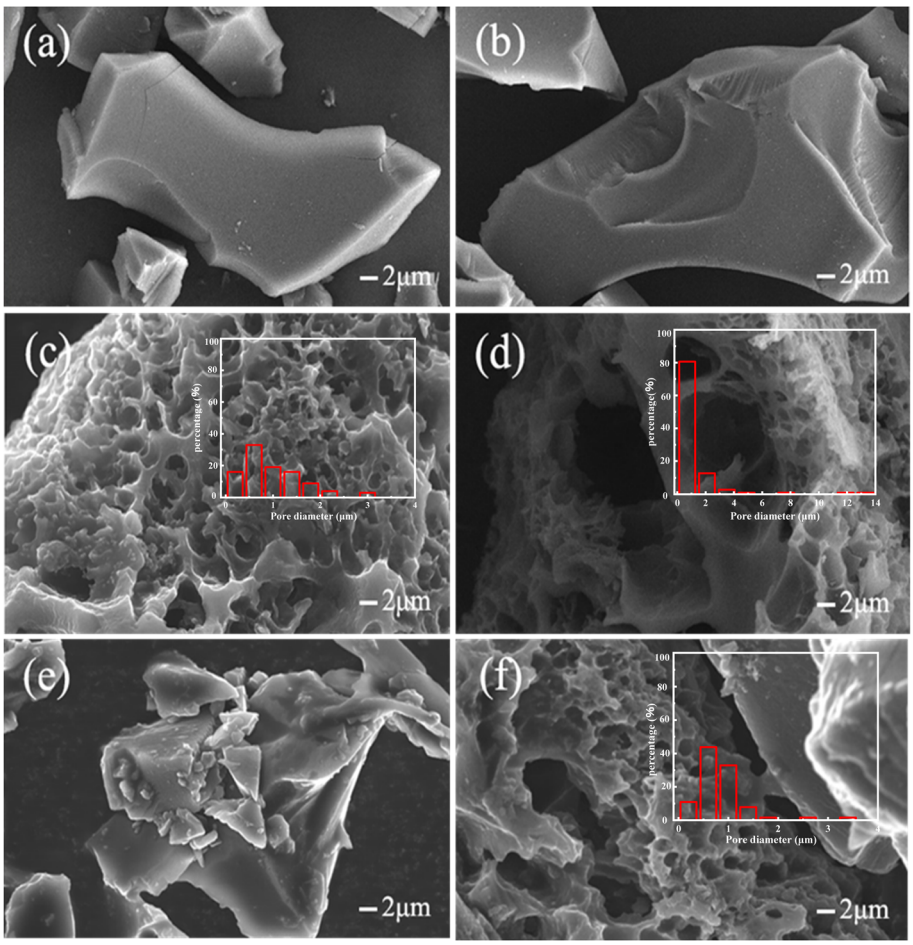


Fig. 1 SEM image of samples: $BC_{2\text{-}400\text{-}4}$ (a); $BC_{2\text{-}600\text{-}4}$ (b); $BC_{2\text{-}800\text{-}4}$ (c); $BC_{2\text{-}1000\text{-}4}$ (d); $BC_{1\text{-}800\text{-}4}$ (e); $BC_{3\text{-}800\text{-}4}$ (f).

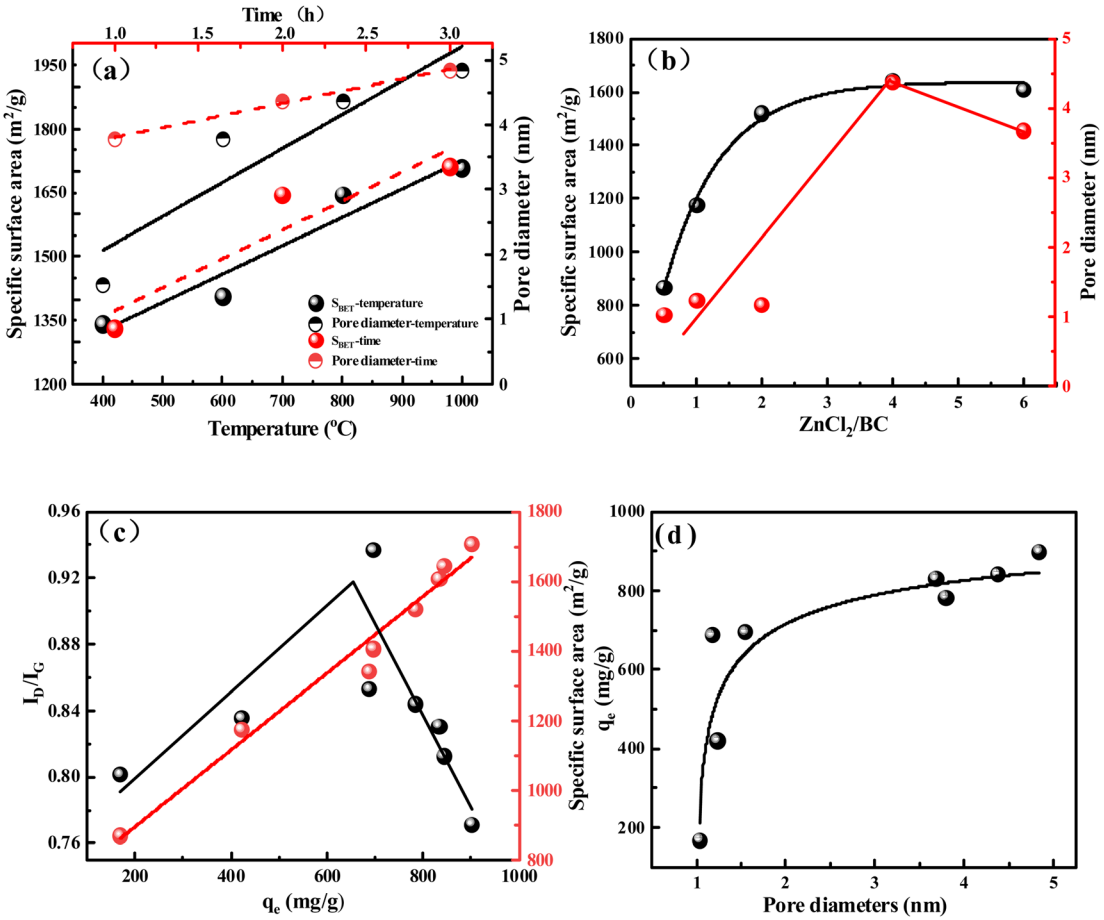


Fig. 2 The effect of $BC_{x\text{-}y\text{-}z}$ temperature and time (a) and the amount of the activator (b) on specific surface area and pore diameter, the effects of specific surface area, $I_D/I_G$ (where $I_D$ and $I_G$ is the D-band and G-band Raman intensity, respectively. The ratio is the ratio of peak intensities) (c), and pore diameter (d) on the $BC_{x\text{-}y\text{-}z}$ adsorption capacity.

structures, where such porous materials have narrow necks and wider openings,[34] which allow TC molecules to enter and exit the pores at different pressures, facilitating mass capture of TC molecules.[32,34]

In order to investigate the effect of preparation conditions on the adsorption properties of biochar and reveal the influence of structure on the adsorption properties, the biochar adsorption properties were evaluated by using antibiotic tetracycline as adsorbate (Fig. 2).

The effects of activation temperature, time, and the amount of the activator on the $BC_{x\text{-}y\text{-}z}$ specific surface area and pore diameter are shown in Fig. 2a and b, respectively. As depicted in Fig. 2a, increasing activation temperature from 400 °C to 800 °C and time from 1 to 3 h, the specific surface area and pore diameter of $BC_{x\text{-}y\text{-}z}$ also increased from 1342 to 1711 $m^2\ g^{-1}$ and 1.54 to 4.84 nm (Table S3†), respectively, displaying a positive correlation. This result indicated that activation temperature and time are favorable for increasing the specific surface area and pore diameter of biochar. As shown in Fig. 2b, the ratio of $ZnCl_2$/starch was improved from 0.5 to 2, and the specific surface area also can increase from 870 to 1521 $m^2\ g^{-1}$ (Table S3†). Then increasing the ratio of $ZnCl_2$/starch from 2 to 6, the surface area change was not obvious. This result indicated that excess $ZnCl_2$ was not effectively involved in the activation process of biochar. Obtained different samples of $BC_{x\text{-}y\text{-}z}$ were used for TC adsorption, showing the best adsorption capacity of about 900.5 mg $g^{-1}$ and the worst adsorption capacity of about 168.25 mg $g^{-1}$ for $BC_{x\text{-}y\text{-}z}$ (Fig. S4†).

What is the reason for the difference in adsorption performance for TC on the surface of biochar? As shown in Fig. 2c, it is easy to find that the adsorption capacity increase with the increasing of special surface area. The specific surface area was increased from 870 $m^2\ g^{-1}$ to 1707 $m^2\ g^{-1}$ (Table S3†), and the adsorption performance was improved from 168.5 mg $g^{-1}$ to 900.5 mg $g^{-1}$ (Fig. S4†). The special surface area has doubled, while the adsorption performance has increased by 5.3 times. It indicates that the large specific surface area is beneficial to adsorb the contaminant.[35] The high surface area of BC provides enormous accessible active sites for the adsorption of TC. As shown in Fig. 2d, the adsorption capacity of micropores is less than 700 mg $g^{-1}$, while the adsorption capacity of mesopores is about 800 mg $g^{-1}$ (Fig. S4†). It is different from the traditional understanding that micropores and mesopores are favorable for the adsorption of contaminants.[35,36] The microporous and

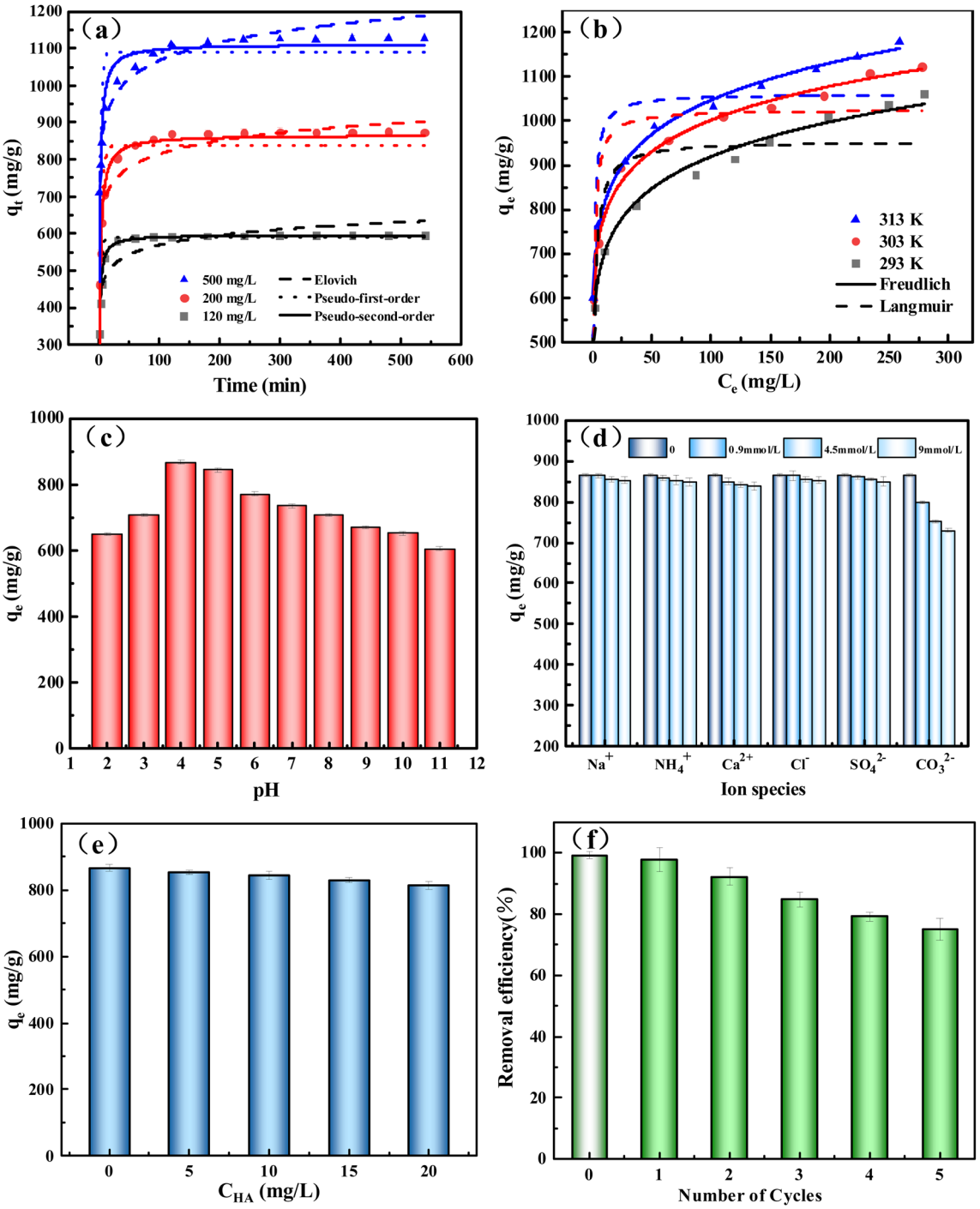


Fig. 3 Kinetic models of pseudo-first-order plots, pseudo-second-order plots, and Elovich plots of $BC_{2\text{-}800\text{-}4}$ for TC adsorption (a); nonlinear Langmuir and Freundlich isotherm models (b); the effect of initial solution pH of $BC_{2\text{-}800\text{-}4}$ on TC removal (c); effects of different ion species of TC adsorption on $BC_{2\text{-}800\text{-}4}$ (d); effects of humic acid on TC adsorption on $BC_{2\text{-}800\text{-}4}$ (e); reusability of $BC_{2\text{-}800\text{-}4}$ for TC adsorption (f).

mesoporous structures on the surface of biochar aren't key factors for the adsorption of TC. Zhu *et al.*[37] found that the presence of micropores has little effect on the adsorption of tetracycline, while Liu *et al.*[38] demonstrated that the adsorption of tetracycline on mesoporous biochar is negatively impacted. In order to further clarify the influence of reaction conditions on the degree of graphitization and to further investigate how the fabrication condition affects the crystallographic structures of BC, we used XRD and Raman to investigate the structural change of BC (Fig. S5†).

The broad diffraction peak at 23.1° in the pattern of BC indicates the amorphous carbon structure of BC (Fig. S5a and b†).[39] As the temperature increased, a new diffraction peak at 43.8° was shown in the curve of BC, which represent graphitic

carbon.[40] After the activation temperature is higher than 600 °C, the graphitization of the biochar can be easily observed in the spectrum. It is not difficult to find that both the activation time and the activation dose have little effect on the peak at 43.6° at 800 °C. Therefore, the most important factor affecting the graphitization of BC is the activation temperature.

Raman spectroscopy was used to measure the change in the degree of graphitization (Fig. S5c and d).† The Raman spectrum of BC shows two highlighted peaks D and G, which are due to the graphite lattice vibration mode and order/disorder in the graphite structure of BC.[18] The peak D indicates disordered $sp^3$-hybridized carbon atoms with vacancies, whereas the peak G represents the extension of $sp^2$ atom pairs in the carbon atom ring.[40] Raman $I_D/I_G$ ratios are applied to assess the quality of carbon materials.[41] It is easy to see that the value of $I_D/I_G$ gradually decreases from 0.9371 to 0.7716 with the increase in activation temperature (Fig. S5c†). The increasing temperatures have a positive influence on forming ordered $sp^2$-hybridized C=C bonds, which implies the formation of the graphitic structure.[42] The $I_D/I_G$ ratios decreased from 0.8898 to 0.8085 (Fig. S5c†) under the same temperature when increasing activation time. After above 2 h, the $I_D/I_G$ ratios presented a trend of slight decrease. $ZnCl_2$ leads to a decrease in $I_D/I_G$ ratio, but this effect is relatively small (Fig. S5d†). There is an aromatic ring in the tetracycline molecule, and the graphitization of $BC_{x\text{-}y\text{-}z}$ is beneficial to the π–π interaction, which improves the adsorption performance. The lower the $I_D/I_G$ value, the higher of the graphitizable degree of carbon material.[43] As shown in Table S3,† $BC_{1\text{-}800\text{-}4}$ and $BC_{2\text{-}400\text{-}4}$ have similar specific surface areas (1331 and 1342 $m^2\ g^{-1}$), but the $I_D/I_G$ value of $BC_{1\text{-}800\text{-}4}$ (0.8898) is lower than that of $BC_{2\text{-}400\text{-}4}$ (0.9371) (Fig. S5c†), indicating that $BC_{1\text{-}800\text{-}4}$ has a higher degree of graphitization. From Fig. S4,† it can be seen that the adsorption capacity of TC on $BC_{1\text{-}800\text{-}4}$ (746 mg $g^{-1}$) is slightly higher than that on $BC_{2\text{-}400\text{-}4}$ (695 mg $g^{-1}$). The same result was obtained for $BC_{3\text{-}400\text{-}4}$ and $BC_{2\text{-}1000\text{-}4}$. This indicates that for biochar with similar specific surface areas, a higher degree of graphitization can slightly promote the adsorption of TC. As shown in Fig. 2c, with increasing the $I_D/I_G$ value from 0.8018 to 0.9371, defects increased, and the adsorption capacity also was enhanced from 168.52 to 695.3 mg $g^{-1}$. At this point, the material has a low specific surface area, which shows that the surface defects of biochar under a low specific surface area are beneficial to improve the adsorption capacity. Moreover, with the decrease of $I_D/I_G$ value from 0.9371 to 0.7716, graphitization is enhanced and adsorption capacity is increased. At this point, the material has a high specific surface area, which shows that the graphitization of biochar surface under a high specific surface area is beneficial to improve the adsorption capacity.

### 3.2 Adsorption performance

**3.2.1 Adsorption kinetics.** The adsorption kinetics, which involves the adsorption mechanism and potential rate control phase, was investigated in detail (Fig. 3a). It was rapid adsorption in the initial 10 min. Then, the adsorption rate gradually decreased. It could be very fast surface adsorption in the initial stage and slow diffusion inside in the second stage.[44] Therefore, it suggests that the special surface area plays a predominant role in the overall adsorption process. The three well-known formulas of pseudo-first-order, pseudo-second-order and Elovich model, and the internal diffusion model were applied to evaluate the adsorption process of TC (Fig. 3a and S6†). The kinetic parameters were shown in Table S3.† All the $R^2$ values of the pseudo-second-order model were above 0.90 and the equilibrium adsorption capacities ($q_e$) were very close to the experimental data, indicating that the adsorption kinetics were well fitted to the pseudo-second-order kinetic model. The adsorption mechanism might involve physisorption.[45,46]

The internal diffusion model was used to investigate the mechanism of adsorption kinetics further. It can be seen from Fig. S6† that the adsorption of TC to $BC_{2\text{-}800\text{-}4}$ is divided into three stages: external diffusion, internal adsorption, and balance.[43] The rate constant ($K_{i1}$ > 87 mg ($g^{-1}$ $min^{-1/2}$)) is the largest in the first stage (Table S4†), which is a rapid adsorption process. It is due to external diffusion, and TC molecules quickly combine with the adsorption sites on the outer surface of $BC_{2\text{-}800\text{-}4}$ from the solution.[9] Then, the effective adsorption site density on the adsorbent decreases in the second stage. TC molecules not only bind with the remaining adsorption sites, but also slowly diffuse into the pores of $BC_{2\text{-}800\text{-}4}$.[47] In the third stage, the adsorption reached equilibrium, and the adsorption reached saturation. All the C values are not zero for all stages. It indicates that intra-particle diffusion is not the controlling factor affecting adsorption in the kinetic process.[48]

**3.2.2 Adsorption isotherm.** Four well-known models, Langmuir, Freundlich, Temkin, and Dubinin–Radushkevich were applied to describe the adsorption isotherm (Fig. 3b, S7, and Table S5†). At low initial concentrations, the adsorption capacity increased rapidly with increasing the concentration of TC. However, the trend of increase was delayed at a high initial concentration. The reason could be that most of the adsorption sites had been occupied, and many TC molecular were difficult to enter the vacancy of the adsorption sites.[49] All the values of $R^2$ were above 0.98, indicating that the Freundlich isotherm model was better than other isotherm models in matching experimental data. The Freundlich adsorption mainly described the multilayer adsorption process for non-uniform surfaces. The value of $1/n_F$ was below 1, implying that the surface of BC had an excellent adsorption affinity.[50] The $R^2$ values of the Temkin model were above 0.96, suggesting that chemisorption existed between $BC_{2\text{-}800\text{-}4}$ and TC, and there is a strong intermolecular force.[51]

In order to evaluate the properties of TC adsorbed by BC, the adsorbent in this work was compared with the reported BC-based adsorbents (Table S6†). For TC adsorbents, $BC_{2\text{-}800\text{-}4}$ has a large specific surface area (1645 $m^2\ g^{-1}$) and a high $q_{max}$ value (1122.2 mg $g^{-1}$). Other activated biochar materials prepared using activators such as NaOH have good adsorption effects.[51] However, their high corrosiveness leads to high preparation costs.[43] Compared with other biochar materials activated by $ZnCl_2$ (*e.g.*, Zn-BC),[11] the adsorption capacity of TC is only 93.44 mg $g^{-1}$. The simple synthesis of $BC_{2\text{-}800\text{-}4}$ and its excellent adsorption performance have broad application promising

 

applications. The only drawback is that the activation temperature is high and the energy consumption is high.

**3.2.3 Adsorption thermodynamics.** The thermodynamic parameters are shown in Table S7.† $\Delta G^0$ is negative growth with the increase of adsorption temperature, which indicates that the high temperature was beneficial to adsorb TC on $BC_{2\text{-}800\text{-}4}$.[43] and $\Delta G^0 < 0$ suggested that the adsorption process was spontaneous. Generally, the absolute values of $\Delta G^0$ between 0 and 20 kJ $mol^{-1}$ indicate physical adsorption, while chemical adsorption is between 80 and 400 kJ $mol^{-1}$.[47] It shows that the adsorption of TC on $BC_{2\text{-}800\text{-}4}$ involves physical adsorption. $\Delta H^0$ and $\Delta S^0 > 0$ suggested that the adsorption of TC by $BC_{2\text{-}800\text{-}4}$ is an endothermic process.[52]

**3.2.4 Effect of pH.** The initial pH of the solution affects the dissociation state of the adsorbent and adsorbate, as well as the force at the adsorption site.[49] Fig. 3c illustrates the TC adsorption properties of $BC_{2\text{-}800\text{-}4}$ at different pH. The maximum adsorption capacity is reached at pH = 4.0. There are two reasons. On the one hand, the surface of $BC_{2\text{-}800\text{-}4}$ was protonated in the acidic solution, and the adsorption capacity of $BC_{2\text{-}800\text{-}4}$ was improved by electrostatic attraction (Fig. 4a). On the other hand, ions such as $TC^+$, $TC^{+-}$, $TC^-$ and $TC^{2-}$ were present in the TC aqueous solution. TC mainly existed in the form of $TC^+$ at pH < 3.4, and $TC^{+-}$ at pH < 7.[53] In the acidic solutions, $H_3O^+$ competed with $TC^+$ to $BC_{2\text{-}800\text{-}4}$ adsorption sites, leading to a small TC adsorption capacity at low pH. As the pH increased, TC in solutions was mainly $TC^{+-}$. The electrostatic attraction between $TC^{+-}$ and the positive charge adsorbents was enhanced, resulting in the adsorption capacity of $BC_{2\text{-}800\text{-}4}$ being improved. In the alkaline solutions, TC mainly existed in the form of $TC^-$ and $TC^{2-}$. BC was denoted negatively charged when the solution pH > 7 (Fig. 4a). Therefore, electrostatic repulsion occurs between BC and $TC^-/TC^{2-}$, resulting in a lower adsorption capacity.

**3.2.5 Effect of coexisting ions.** Both natural and waste waters are rich in various inorganic anions and cations, which can compete with TC for adsorption sites and therefore affect the removal efficiency of $BC_{2\text{-}800\text{-}4}$. In this study, we selected six typical coexisting ions ($Na^+$, $NH_4^+$, $Ca^{2+}$, $Cl^-$, $SO_4^{2-}$, $CO_3^{2-}$) to investigate their impact on the adsorption of TC by $BC_{2\text{-}800\text{-}4}$. $Na^+$, $NH_4^+$, $Ca^{2+}$, $Cl^-$ and $SO_4^{2-}$ have little effect on the removal of TC, and $q_e$ remained above 840 mg $g^{-1}$ in 9 mmol $L^{-1}$ interference ions ($C_{TC}$ = 0.9 mmol $L^{-1}$) (Fig. 3d). $CO_3^{2-}$ has a great effect on the adsorption capacity. The main reason is that the pH of the solution increases with the addition of $Na_2CO_3$, which increases the electrostatic repulsion between $BC_{2\text{-}800\text{-}4}$ and TC (Fig. 4b).[43] As a result of the decomposition of natural organic compounds, natural organic matter such as humic acid (HA) is widely present in aquatic environments, which may affect the removal of TC. Therefore, this experiment investigated the influence of HA at concentrations of 5–20 mg $L^{-1}$ on the adsorption of TC by $BC_{2\text{-}800\text{-}4}$. The results are shown in Fig. 3e. HA has a slight impact on the adsorption capacity. The zero-charge point of HA is about pH = 2.0.[54] It is a negatively charged form at pH = 4, which can be attracted by $BC_{2\text{-}800\text{-}4}$ through electrostatic interaction and compete with TC for the adsorption site. In addition, HA is a macromolecule with abundant functional groups, which may react with TC molecules and form complex surface complexation.[55] This is unfavorable to the adsorption of TC.

**3.2.6 Reusability.** The results of cyclic adsorption of the TC by $BC_{2\text{-}800\text{-}4}$ is shown in Fig. 3f. The TC removal efficiencies could be up to nearly 100% in the first cycle. After 5 cycles, the TC removal efficiency is still higher than 75%. It indicates that $BC_{2\text{-}800\text{-}4}$ has good desorption efficiency and excellent TC adsorption performance. It confirmed the effectiveness of $BC_{2\text{-}800\text{-}4}$ in the adsorption of the TC in recycling applications.

### 3.3 Adsorption mechanism

The investigation of the adsorption mechanism is of great significance to the understanding of the adsorption process. The adsorbent that reached the equilibrium state of adsorption was filtered and collected, and then dried in an oven at 60 °C for 12 h to obtain the adsorbed adsorbent. The structure of $BC_{2\text{-}800\text{-}4}$ before and after adsorption was determined to elucidate the adsorption mechanism. The results are shown in Fig. 5.

The specific surface area dropped sharply from 1645 $m^2$ $g^{-1}$ before adsorption to 512 $m^2$ $g^{-1}$ after adsorption, indicating that a large amount of TC occupies the surface and pores of $BC_{2\text{-}800\text{-}4}$ (Fig. 5a).[56] Through the analysis of pore structure, we can find that the pore size decreases from 4.37 nm to 3.82 nm (after adsorption), and the pore volume decreases from 1.72 $m^3$ $g^{-1}$ to

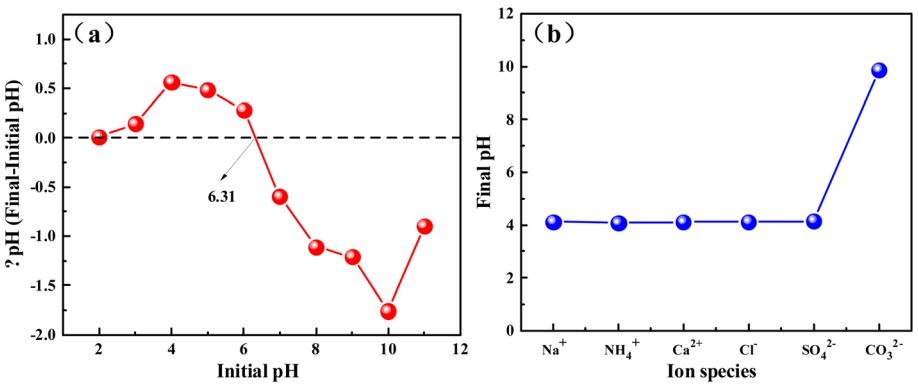


Fig. 4 pHpzc of biochar $BC_{2\text{-}800\text{-}4}$ (a); the pH after adsorption in coexisting ions solution (b).

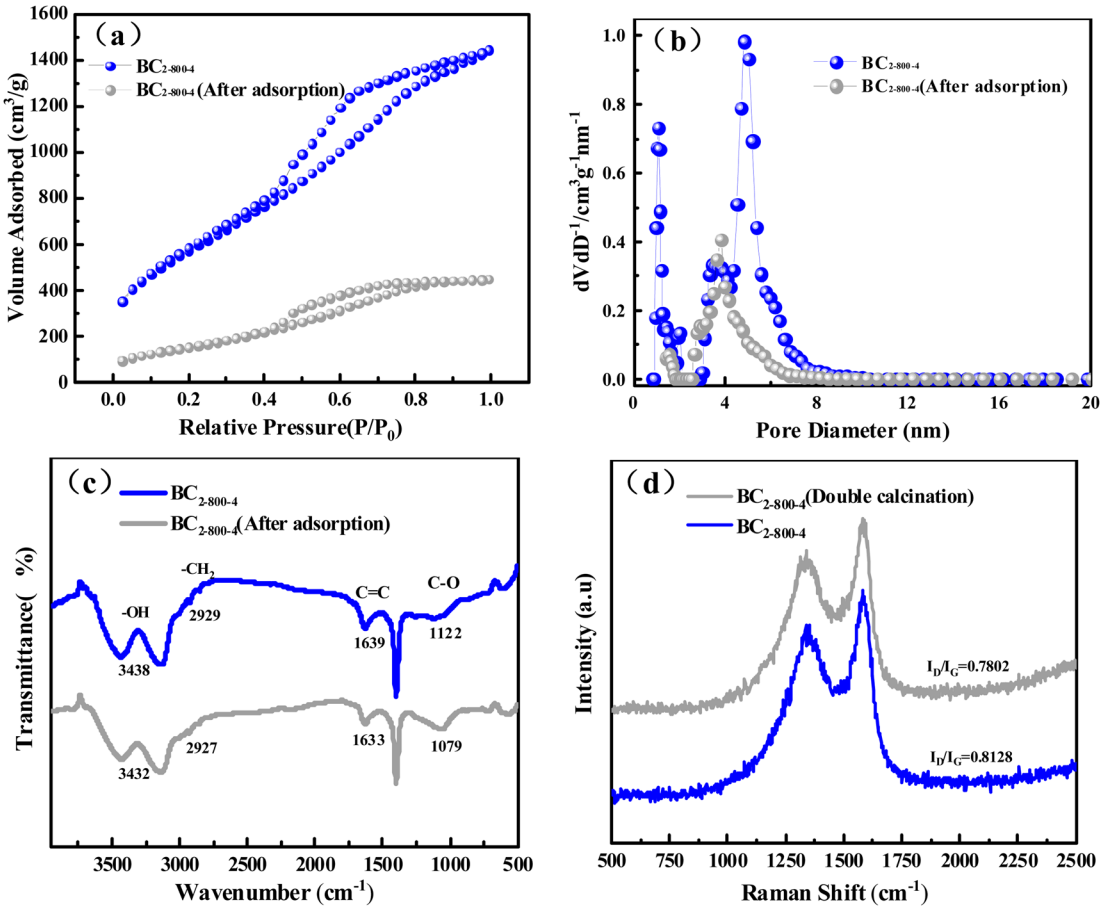


Fig. 5 $N_2$ adsorption–desorption isotherms (a) and the pore-size distribution curve (b) of $BC_{2\text{-}800\text{-}4}$ before and after adsorption, FTIR spectra (c) of $BC_{2\text{-}800\text{-}4}$ before and after adsorption, annealing experiment of $BC_{2\text{-}800\text{-}4}$ (d).

0.68 $m^3\ g^{-1}$ (after adsorption) (Fig. 5b). This proves that TC is effectively adsorbed into the surface and pores of $BC_{2\text{-}800\text{-}4}$.

The infrared spectra showed that the stretching vibration peak of the adsorbent at 3438 $cm^{-1}$ was reduced to 3432 $cm^{-1}$ (Fig. 5c). It indicates hydroxy protonation shifts due to electrostatic interaction and hydrogen bond formation between hydroxyl and amino groups of tetracycline and oxygen-containing functional groups of $BC_{2\text{-}800\text{-}4}$.[18,57] The peak at 1639 $cm^{-1}$, which is the vibration of C=C, also shifted after adsorption. It is attributed to the π–π conjugate effect between the π electron enrichment region of $BC_{2\text{-}800\text{-}4}$ and the aromatic ring in TC molecule.[58]

In order to compare the π–π interaction with the hydrogen bond force, the BC was calcined again at 800 °C for 2 h to reduce the –OH content in the $BC_{2\text{-}800\text{-}4}$ (Fig. 5d). The results show that the degree of graphitization is higher ($I_D/I_G$ = 0.7802 < 0.8128) and the adsorption capacity increased from 867 mg $g^{-1}$ to 911 mg $g^{-1}$. This shows that the contribution of the hydroxyl group is weaker than that of π–π interaction.

All density functional theory (DFT) calculations in this work were performed using Gaussian 09 program package.[59] A polarized continuum model based on solute electron density (PCM-SMD)[60,61] was employed to simulate the solvent effect of aqueous solution. The dispersion corrections were computed with Grimme's D3 (BJ) method in optimization.[62] Full geometry optimizations were operated to locate all of the stationary points, using B3LYP density functional theory method with 6-31G(d) basis set for all atoms,[63,64] namely, B3LYP/6-31G(d). Unless mentioned otherwise, the relative energies ($\Delta G$, kJ $mol^{-1}$) are relative to the initial reactants obtained at the B3LYP/6-31G(d) + PCM-SMD (water) level in aqueous solution under experimental temperature and pressure (298.15 K and 1 atm).

DFT calculations were carried out to verify the adsorption of TC over BC (graphene sheet $C_{42}H_{16}$ terminated by hydrogen atoms). Analysis of the wave function indicates that the electron absorption corresponds to the transition from the ground to the first excited state and is mainly described by one-electron excitation from the highest occupied molecular orbital (HOMO) to the lowest unoccupied molecular orbital (LUMO). The HOMO and LUMO are delocalized over the entire C=C bond of BC, as depicted in Fig. 6a. Obviously, the HOMO and LUMO are delocalized over the entire C=C bond of the benzene ring and oxygen atom of –OH group for TC in Fig. 6b. Consequently, the lone pair electron on 2p orbital of carbon atoms for BC spontaneously matches with the 2p orbital of the oxygen atom and the benzene ring for TC, resulting in such strong π–π stacking interaction and p–π stacking interaction from C=C bond of

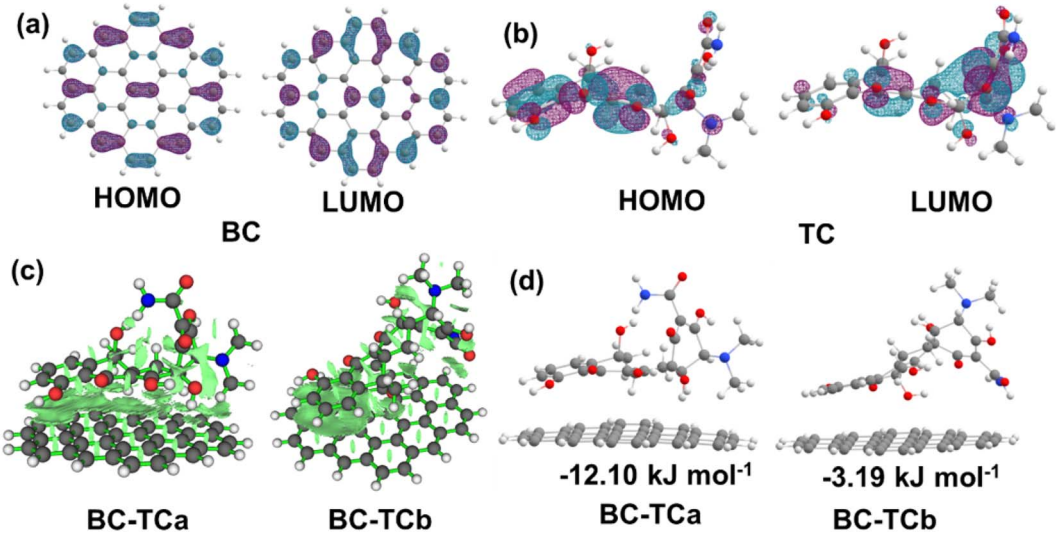


Fig. 6 (a) and (b) The visualization of the characteristic molecular orbital for BC and TC, respectively. (c) The weak interaction of BC-TCa and BC-TCb visualized using Multiwfn software.[65] (d) Optimized geometric structures of BC with the TC adsorption mode.

benzene ring for BC to C=C bond of benzene ring for TC and to the oxygen atom of –OH group for TC in BC-TCa, but in the adsorption BC-TCb structure only strong π–π stacking interaction, as shown in Fig. 6c. The positive adsorption free energy −12.10 and −3.19 kJ mol$^{-1}$ of BC-TCa and BC-TCb, respectively, indicates that the product tends to desorb from the BC adsorbent. The adsorption-free energy of BC-TCa is greater than that of BC-TCb, which indicates that strong π–π stacking interaction and p–π stacking interaction can enhance the adsorption effect from BC to TC, compared to π–π stacking interaction. This result is consistent with the experimental results.

In summary, the adsorption mechanism of TC in aqueous solutions by BC can be visualized as follows: (1) the special surface area and pore structure of BC is critical to the removal of TC. (2) The π–π stacking interaction and p–π stacking interaction play an important role in the adsorption of TC. (3) Electrostatic attraction and hydrogen bonding also play an indispensable role in the adsorption of TC.

## 4 Conclusion

Corn starch-based biochar was prepared with $ZnCl_2$ as an activator. Zinc chloride and starch were activated at 800 °C for 2 hours at a weight ratio of 4 : 1 to obtain porous graphite biochar $BC_{2\text{-}800\text{-}4}$ with an ultra-large surface area. The initial pH, contact time, TC concentration, temperature, and interference ions influenced TC removal to some degree. The maximum adsorption capacity could get 1122.2 mg g$^{-1}$ at room temperature. The pseudo-second-order and Freundlich models could better explain the kinetics and equilibrium, respectively. The adsorption mechanism of TC on $BC_{2\text{-}800\text{-}4}$ included electrostatic attraction, π–π, and p–π interactions, pore-filling, and hydrogen bonding. The surface defects and small surface area of biochar synergistically enhance the adsorption activity of tetracycline. Biochar with ultra-large surface area promotes the activity of TC, while the defects are the opposite. The effect of mesoporous materials with ultra-large specific surface area and graphitic degree on the removal of TC provides a reliable way for the removal of TC pollutants in water by BC.

## Conflicts of interest

There are no conflicts to declare.

## Acknowledgements

This work was supported by the Sichuan Science and Technology Program, China (2022NSFSC0350), the application Technology Research and Development Special Project of Nanchong, China (21YFZJ0109), Key Laboratories of Fine Chemicals and Surfactants in Sichuan Provincial Universities (2021JXY01).

## References

1 Z. Wang, Y. Du, C. Yang, X. Liu, J. Zhang, E. Li, Q. Zhang and X. Wang, *Sci. Total Environ.*, 2017, **609**, 1423–1432.
2 S. Liu, M. Pan, Z. Feng, Y. Qin, Y. Wang, L. Tan and T. Sun, *New J. Chem.*, 2020, **44**, 1097–1106.
3 R. V. Xikhongelo, F. M. Mtunzi, P. N. Diagboya, B. I. Olu-Owolabi and R.-A. Düring, *Ind. Eng. Chem. Res.*, 2021, **60**, 3957–3968.
4 A. M. Pandele, H. Iovu, C. Orbeci, C. Tuncel, F. Miculescu, A. Nicolescu, C. Deleanu and S. I. Voicu, *Sep. Purif. Technol.*, 2020, **249**, 117145.
5 W. Chen, B. Zhao, Y. Guo, Y. Guo, Z. Zheng, T. Pak and G. Li, *J. Environ. Chem. Eng.*, 2021, **9**, 106557.
6 J. Cao, S. Sun, X. Li, Z. Yang, W. Xiong, Y. Wu, M. Jia, Y. Zhou, C. Zhou and Y. Zhang, *Chem. Eng. J.*, 2020, **382**, 122802.

7 S. Wu, H. Hu, Y. Lin, J. Zhang and Y. H. Hu, *Chem. Eng. J.*, 2020, **382**, 122152.
8 J. Liu, B. Zhou, H. Zhang, J. Ma, B. Mu and W. Zhang, *Bioresour. Technol.*, 2019, **294**, 122152.
9 P. Zhang, Y. Li, Y. Cao and L. Han, *Bioresour. Technol.*, 2019, **285**, 121348.
10 Y. Dai, J. Li and D. Shan, *Chemosphere*, 2020, **238**, 124432.
11 L. Yan, Y. Liu, Y. Zhang, S. Liu, C. Wang, W. Chen, C. Liu, Z. Chen and Y. Zhang, *Bioresour. Technol.*, 2020, **297**, 122381.
12 C. Senthil and C. W. Lee, *Renewable Sustainable Energy Rev.*, 2021, **137**, 110464.
13 H. M. Jang and E. Kan, *Bioresour. Technol.*, 2019, **274**, 162–172.
14 J. Zhao, F. Gao, Y. Sun, W. Fang, X. Li and Y. Dai, *J. Environ. Chem. Eng.*, 2021, **9**, 105585.
15 J. E. Kim, S. K. Bhatia, H. J. Song, E. Yoo, H. J. Jeon, J. Y. Yoon, Y. Yang, R. Gurav, Y. H. Yang, H. J. Kim and Y. K. Choi, *Bioresour. Technol.*, 2020, **306**, 123092.
16 J. Scaria, K. V. Anupama and P. V. Nidheesh, *Sci. Total Environ.*, 2021, **771**, 145291.
17 X. Sheng, J. Wang, Q. Cui, W. Zhang and X. Zhu, *Environ. Res.*, 2022, **207**, 112175.
18 J. Hoslett, H. Ghazal, E. Katsou and H. Jouhara, *Sci. Total Environ.*, 2021, **751**, 141755.
19 J. Chen, H. Li, J. Li, F. Chen, J. Lan and H. Hou, *J. Mol. Liq.*, 2021, **340**, 117237.
20 H. M. Jang, S. Yoo, Y. K. Choi, S. Park and E. Kan, *Bioresour. Technol.*, 2018, **259**, 24–31.
21 H. Fu, K. Huang, G. Yang, Y. Cao, H. Wang, F. Peng, X. Cai, H. Gao, Y. Liao and H. Yu, *ACS Catal.*, 2021, **11**, 8872–8880.
22 Q. Zheng, B. Huang, X. Du, J. Zhang, H. Fu, H. Gao and Y. Liao, *J. Environ. Chem. Eng.*, 2023, **11**, 109125.
23 S. Wang, S. Ai, C. Nzediegwu, J. H. Kwak, M. S. Islam, Y. Li and S. X. Chang, *Bioresour. Technol.*, 2020, **309**, 123390.
24 T. Chen, L. Luo, S. Deng, G. Shi, S. Zhang, Y. Zhang, O. Deng, L. Wang, J. Zhang and L. Wei, *Bioresour. Technol.*, 2018, **267**, 431–437.
25 H. M. Jang and E. Kan, *Bioresour. Technol.*, 2019, **284**, 437–447.
26 S. Niazi, E. Olsen and H. S. Nygård, *J. Mol. Liq.*, 2020, **317**, 114069.
27 Y. Du, H. Chen, X. Xu, C. Wang, F. Zhou, Z. Zeng, W. Zhang and L. Li, *Microporous Mesoporous Mater.*, 2020, **293**, 109831.
28 Y. Huang, Z. Liu and G. Zhao, *RSC Adv.*, 2016, **6**, 78909–78917.
29 K. A. Addey, *Food Energy Secur.*, 2020, **10**, e265.
30 D. Wei, H. H. Ngo, W. Guo, W. Xu, B. Du, M. S. Khan and Q. Wei, *Bioresour. Technol.*, 2018, **249**, 410–416.
31 K. Ding, X. Zhou, H. Hadiatullah, Y. Lu, G. Zhao, S. Jia, R. Zhang and Y. Yao, *J. Hazard. Mater.*, 2021, **420**, 126551.
32 M. Thommes, K. Kaneko, A. V. Neimark, J. P. Olivier, F. Rodriguez-Reinoso, J. Rouquerol and K. S. W. Sing, *Pure Appl. Chem.*, 2015, **87**, 1051–1069.
33 Q. Wu, Y. Zhang, M. H. Cui, H. Liu, H. Liu, Z. Zheng, W. Zheng, C. Zhang and D. Wen, *J. Hazard. Mater.*, 2022, **426**, 127798.
34 S. Seo, W. Chaikittisilp, N. Koike, T. Yokoi and T. Okubo, *Microporous Mesoporous Mater.*, 2019, **278**, 212–218.
35 A. C. Martins, O. Pezoti, A. L. Cazetta, K. C. Bedin, D. A. S. Yamazaki, G. F. G. Bandoch, T. Asefa, J. V. Visentainer and V. C. Almeida, *Chem. Eng. J.*, 2015, **260**, 291–299.
36 J. Yang, J. Dai, L. Wang, W. Ge, A. Xie, J. He and Y. Yan, *J. Taiwan Inst. Chem. Eng.*, 2019, **96**, 473–482.
37 X. Zhu, C. Li, J. Li, B. Xie, J. Lu and Y. Li, *Bioresour. Technol.*, 2018, **263**, 475–482.
38 Y. Liu, W. Gao, S. Yin, R. Liu and Z. Li, *Front. Chem.*, 2022, **10**, 1078877.
39 K. Li, S. Ma, S. Xu, H. Fu, Z. Li, Y. Li, S. Liu and J. Du, *J. Hazard. Mater.*, 2021, **404**, 124145.
40 B. Li, Y. Huang, Z. Wang, J. Li, Z. Liu and S. Fan, *Environ. Sci. Pollut. Res. Int.*, 2021, **28**, 44140–44151.
41 B. Prakoso, Y. Ma, R. Stephanie, N. H. Hawari, V. Suendo, H. Judawisastra, Y. Zong, Z. Liu and A. Sumboja, *RSC Adv.*, 2020, **10**, 10322–10328.
42 X. Wei, R. Zhang, W. Zhang, Y. Yuan and B. Lai, *RSC Adv.*, 2019, **9**, 39355–39366.
43 Z. Zhang, Y. Li, L. Ding, J. Yu, Q. Zhou, Y. Kong and J. Ma, *Bioresour. Technol.*, 2021, **330**, 124949.
44 W. Liu, X. Liu, J. Chang, F. Jiang, S. Pang, H. Gao, Y. Liao and S. Yu, *Front. Chem. Sci. Eng.*, 2021, **15**, 1185–1196.
45 Y. Liao, S. Chen, Q. Zheng, B. Huang, J. Zhang, H. Fu and H. Gao, *Front. Chem. Sci. Eng.*, 2022, **139**, 109341.
46 J. Su, H.-f. Lin, Q.-P. Wang, Z.-M. Xie and Z.-l. Chen, *Desalination*, 2011, **269**, 163–169.
47 H. Yu, L. Gu, L. Chen, H. Wen, D. Zhang and H. Tao, *Bioresour. Technol.*, 2020, **316**, 123971.
48 X. Fang, J. Zou, N. Ma and W. Dai, *Langmuir*, 2022, **38**, 14451–14464.
49 W. Wang, M. Gao, M. Cao, X. Liu, H. Yang and Y. Li, *Bioresour. Technol.*, 2021, **332**, 125059.
50 Y. Zhu, D. Wu, J. Chen, N. Ma and W. Dai, *J. Solid State Chem.*, 2023, **319**, 123797.
51 J. Dai, X. Meng, Y. Zhang and Y. Huang, *Bioresour. Technol.*, 2020, **311**, 123455.
52 Y. Jia, L. Ding, P. Ren, M. Zhong, J. Ma and X. Fan, *J. Chem. Eng. Data*, 2020, **65**, 725–736.
53 X. Zhang, Y. Li, M. Wu, Y. Pang, Z. Hao, M. Hu, R. Qiu and Z. Chen, *Bioresour. Technol.*, 2021, **320**, 124264.
54 H. Peng, J. Cao, W. Xiong, Z. Yang, M. Jia, S. Sun, Z. Xu, Y. Zhang and H. Cai, *J. Hazard. Mater.*, 2021, **402**, 123498.
55 Y. Li, S. Wang, Y. Zhang, R. Han and W. Wei, *J. Mol. Liq.*, 2017, **247**, 171–181.
56 R. Ocampo-Pérez, J. Rivera-Utrilla, C. Gómez-Pacheco, M. Sánchez-Polo and J. J. López-Peñalver, *Chem. Eng. J.*, 2012, **213**, 88–96.
57 Z. Zeng, S. Ye, H. Wu, R. Xiao, G. Zeng, J. Liang, C. Zhang, J. Yu, Y. Fang and B. Song, *Sci. Total Environ.*, 2019, **648**, 206–217.
58 H. Zhou, X. Li, H. Jin and D. She, *Bioresour. Technol.*, 2022, **346**, 126652.
59 G. W. M. J. T. Frisch, H. B. Schlegel, G. E. Scuseria, M. A. Robb, J. R. Cheeseman, G. Scalmani, V. Barone,

B. Mennucci, G. A. Petersson, *et al.*, Revision C.01, Gaussian Inc., Wallingford, CT, 2010.
60 M. Cossi, G. Scalmani, N. Rega and V. Barone, *J. Chem. Phys.*, 2002, **117**, 43–54.
61 A. V. Marenich, C. J. Cramer and D. G. Truhlar, *J. Phys. Chem. B*, 2009, **113**, 6378–6396.
62 S. Grimme, J. Antony, S. Ehrlich and H. Krieg, *J. Chem. Phys.*, 2010, **132**, 154104.
63 R. Krishnan, J. S. Binkley, R. Seeger and J. A. Pople, *J. Chem. Phys.*, 1980, **72**, 650–654.
64 A. D. McLean and G. S. Chandler, *J. Chem. Phys.*, 1980, **72**, 5639–5648.
65 T. Lu and F. Chen, *J. Comput. Chem.*, 2012, **33**, 580–592.